Dyes and Pigments 225 (2024) 112053

Contents lists available at ScienceDirect

Dyes and Pigments

journal homepage: www.elsevier.com/locate/dyepig

Quinoline-based hydrazones for biocide detection: Machine learning-aided design of new TBT chemosensors

Rui P.C.L. Sousa , Filipe Teixeira , Susana P.G. Costa , Rita B. Figueira , M. Manuela M. Raposo *

Centre of Chemistry, University of Minho, Campus of Gualtar, 4710-057, Braga, Portugal

A R T I C L E I N F O

Keywords:
Tributyltin (TBT)
Biocide
Optical chemosensor
Hydrazone
Thiosemicarbazone
Quinoline

A B S T R A C T

Antifouling compounds are used as paint components to mitigate biofouling on ships and submerged structures. One of the most known and used antifouling compounds is tributyltin (TBT). However, TBT is toxic to aquatic living beings, causing problems such as reduction of growth and *imposex*. The development of a TBT chemosensor could be of utter relevance in the building of an *in-situ* TBT monitoring device. Therefore, this work reports the synthesis of five new quinoline-based hydrazones (HZ) and two new quinoline-based thiosemicarbazones (TSC), with synthesis yields from 17 to 83 %. The compounds were tested in the presence of TBT, and some compounds of the group showed colorimetric or fluorimetric changes. The interaction between these compounds and TBT was tested by spectrophotometric or spectrofluorimetric titrations, which allowed to calculate the limit of detection (LOD) for each interaction. The fluorimetric interaction between HZ **4a** and TBT was shown to be the most sensitive chemosensory method, with a LOD value of 1.7 μM.

A Ridge classifier model was developed to correlate the ability for TBT detection and the modification of the structure of each molecule. The validity of the proposed model was tested by assessing the TBT-sensing ability of the two novel TSC **5a** and **5b**, which were synthesized after the development of the model. These two compounds also showed colorimetric changes in the presence of TBT, with LODs of 13.8 and 3.1 μM, respectively, in good accordance with the model's predictions. Further analysis of the model's decision process provided some insights on the desirable properties of the novel quinoline-derived TBT optical chemosensors.

1. Introduction

Biofouling can be defined as the accumulation of microorganisms, algae, or small plants on submerged structures such as ships and vessels' hulls or offshore structures. This problem affects these structures not only by direct degradation by microbially induced corrosion [1,2], but also indirectly by impacting the hydrodynamic performance (thus affecting the fuel consumption of ships and vessels), or even by reallocation of microorganisms from one region to another such as in the case of mobility of offshore structures [1–9]. The fuel consumption increase is a particularly important factor due to the rise of the costs and pollution that it involves [4–6]. Therefore, antifouling paints are used worldwide, mainly in the naval industry, to mitigate the problematic of biofouling.

Tributyltin (TBT) is an organotin cationic compound and one of the most used biocides for the aforementioned purpose. In the 1980s, approximately 80% of the naval transport vessels used TBT-based antifouling paints due to their high efficiency [3,4,10]. However, this compound was found to be acutely toxic to aquatic environments due to the leaching from the submerged structures. TBT is absorbed by microorganisms and then incorporated in the tissues of higher organisms by bioaccumulation [11–14]. High TBT concentrations can induce a reduction in the growth and in the long-term survival of several species. Also, a correlation between TBT levels and *imposex*, the superimposition of male sexual characteristics on female marine gastropods, was established [15,16]. The bioaccumulation of TBT results in higher testosterone levels and may cause an endocrine disrupting effect [17].

In 2008, the Rotterdam Convention banned the use of organotins as biocides in antifouling paints. However, some countries have not signed this convention and TBT effects are still impacting aquatic environments. Despite the ban on TBT, the impact of this pollutant is still widespread, not only in the countries that did not sign the convention but also on other parts of the world [18–20]. TBT monitoring is currently approached by sampling and laboratory analysis using chromatographic techniques, such as Liquid Chromatography-Mass Spectrometry (LC-MS) and Gas Chromatography-Mass Spectrometry (GC-MS). These methods

* Corresponding author.
E-mail address: mfox@quimica.uminho.pt (M.M.M. Raposo).

https://doi.org/10.1016/j.dyepig.2024.112053
Received 26 September 2023; Received in revised form 7 February 2024; Accepted 23 February 2024
Available online 25 February 2024

require long procedures with several steps, such as extraction, pre-concentration, and derivatization, besides the need for advanced equipment, expert users, and the high costs of all the procedure. The development of a TBT chemosensor would allow *in-situ* sensing of this biocide. As far as the authors are concerned, there is only one report of an organic probe for TBT recognition. Jin and collaborators synthesized rhodamine-based probes, functionalized with a hydrazone moiety [21]. The new fluorimetric probes were able to detect and quantify TBT between 6 and 20 μM. The cavity formed around the two nitrogen atoms from the hydrazone moiety and an adjacent carbonyl group was the proposed binding site for TBT.

It is undeniable that hydrazones (HZ) are a family of molecules with particular interest in the design of chemosensors. The hydrazone group between the π-conjugated (hetero)aromatic moieties can act as the binding cavity with tuneable sizes. Within this group, thiosemicarbazones (TSC) are a specific type of HZ that can provide extra heteroatoms that can be involved in the chelation of a specific analyte. Both HZ and TSC are widely used in the chemosensing field, with reports of sensors towards metallic cations, small molecules, or organic anions [22–28].

Herein, the authors report the synthesis of five new quinoline-based HZ and two new quinoline-based TSC (see Scheme 1). The compounds were synthesized by simple condensation reactions and with no purification required after precipitation from the reaction mixture, in yields ranging from 17 to 83 %. The seven novel compounds, together with two other previously reported quinoline-based HZ [29], and the two quinoline precursors, were tested in the presence of TBT. After preliminary chemosensory tests, the compounds that showed colorimetric or fluorimetric changes in the presence of TBT were submitted to spectrophotometric or spectrofluorimetric titrations with the biocide. The results from these surveys were fed to a structure-property classification model using readily available electronic descriptors derived from quantum mechanical calculations to these novel compounds. The validity of the proposed model was tested by evaluating the possible TBT-sensing ability of the two TSC compounds prior to their synthesis. Further insights on the discrimination between sensing and non-sensing compounds were assessed from the model in order to gain some insights into desirable structural properties of novel TBT-sensing molecules.

2. Materials and methods

2.1. Materials

Melting points were measured on a Stuart SMP3 melting point apparatus. TLC analysis was carried out on 0.20 mm thick precoated silica plates (Macherey-Nagel), and spots were visualized under UV light on a CN-15 camera (Vilber Lourmat). Chromatography on silica gel was carried out on Acros Organics silica gel 60 (0.035–0.070 mm). Infrared spectra were obtained on a PerkinElmer Spectrum Two instrument with ATR accessory, in the 450-4000 cm^{-1} range with 32 scans. The solid compound was applied directly on the ATR crystal with pressure applied with the incorporated press. UV–Vis absorption spectra (200–700 nm) were obtained using Shimadzu UV/3101 PC spectrophotometer and fluorescence spectra with Fluoromax-4 spectrofluorometer. NMR spectra were obtained on a Bruker Avance III 400 at an operating frequency of 400 MHz for ^{1}H and 100.6 MHz for ^{13}C using the solvent peak as internal reference at 25 °C. All chemical shifts are given in ppm using δ_H $Me_4Si = 0$ ppm as reference and *J* values are given in Hz. Assignments were supported by spin decoupling double resonance and bidimensional heteronuclear correlation techniques. High-resolution mass spectrometry analysis was performed on a QqTOF Impact IITM mass spectrometer (Bruker Daltonics) at the Mass Spectrometry Facility (CQE - IST Node Campus Alameda, Lisboa, Portugal). All commercial reagents and solvents were used as received.

2.2. General procedure for the synthesis of heterocyclic quinoline-based hydrazones and thiosemicarbazones

Equimolar amounts (0.318 mmol) of the appropriate hydrazine or thiosemicarbazide and quinoline-based aldehyde were dissolved in 10 mL of MeOH at room temperature. The reaction mixtures were stirred for 8–10 h. The precipitated compounds were isolated by filtration and then dried in the oven at 40 °C overnight. No additional purification was required. The characterization details are given in Supporting Information.

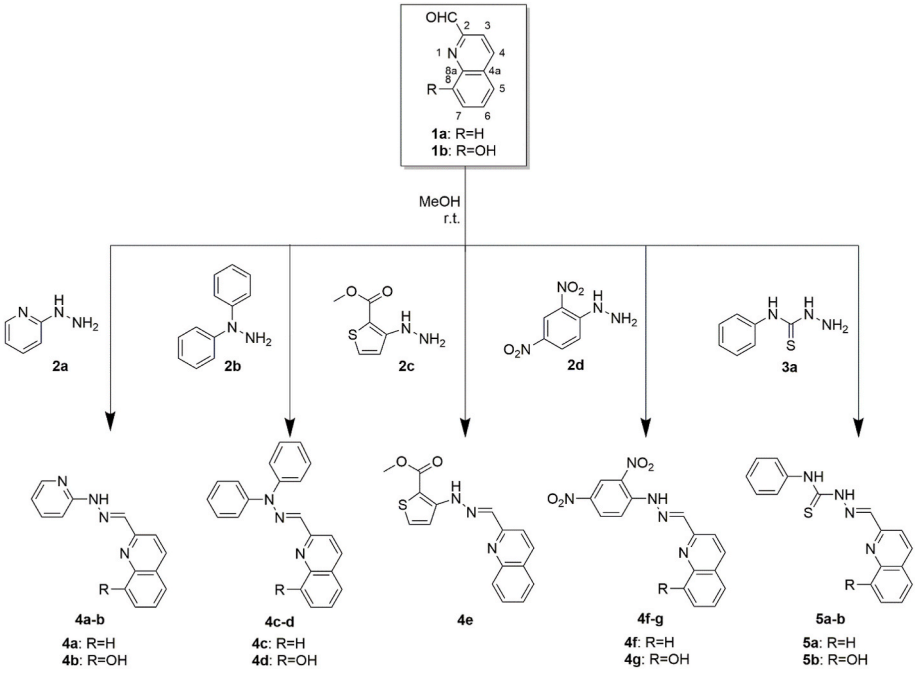

Scheme 1. Synthesis of quinoline-based hydrazones **4a-g** and thiosemicarbazones **5a-b**.

2.3. Chemosensory studies

In the preliminary studies, 50 equivalents (50 μL) of each ion (1×10^{-2} M) were added to an ACN solution of each compound (1 mL, 1×10^{-5} M). The evaluation of color/fluorescence changes was evaluated by naked eye and in a UV–vis chamber under ultraviolet light at 312 nm. Spectrophotometric and spectrofluorimetric titrations were performed when an interaction between compound and ion was seen. To an ACN solution of each compound (3 mL, 1×10^{-5} M), a sequential addition of each ion (1×10^{-2} M) was performed, and the absorbance/fluorescence spectra were analyzed until the plateau was reached. The limit of detection (LOD) and limit of quantification (LOQ) were calculated with the slope of the linear zone of the calibration curve [30].

2.4. Computational methods

The molecular structure of each quinoline or hydrazone molecule was optimized using Density Functional Theory (DFT) at the B3LYP [31] approximation and using the Def2-TZVP basis set [32], as well as the semi-empirical D3 dispersion corrections with Becke-Johnson damping (D3BJ) [33,34], as implemented in the Orca software package, version 5.0.3 [35]. The true minima nature of the optimized geometries was confirmed by the lack of imaginary vibrational frequencies. All structures were then analyzed under the formalism of Bader's Quantum Theory of Atoms In Molecules (QTAIM), using MultiWFN, version 3.8 [36].

The data collected from these calculations was then feed onto a Ridge Regression classifier algorithm, as implemented in the scikit-learn package version 1.1.3 [37], in order to train a small predictive model of the chemosensing ability of these compounds. This was accomplished in a two-stage manner: a preliminary model was first trains using all the collected data: HOMO and LUMO energies and delocalization indexes; Shannon's aromaticity index [38] of the quinoline moiety; QTAIM charges of the quinoline atoms, as well as their respective average and standard deviation; delocalization index between adjacent atoms of the quinoline moiety; weight of the atomic contributions of each quinoline atom to the HOMO or LUMO; total QTAIM charge of the quinoline moiety, Pearson's chemical hardness, the electronic chemical potential, and the global electrophilicity power. A permutation importance routine [39] was then established to determine the most important features of the preliminary model. The twelve most important features of the preliminary model were then used to train the final Ridge classifier model. Further analysis of the final model was carried out using the SHAP framework [40,41].

3. Results and discussion

3.1. Synthesis of quinoline-based hydrazones

A new group of HZ was designed to be tested as TBT chemosensors. This type of compound shows promising structural characteristics for the design of chemosensors, due to the electrophilic and nucleophilic character of imine carbon [22,23,25,42–45]. The triatomic structure C=N–N possesses a configurational isomerism stemming from the intrinsic nature of the C=N double bond, which can contribute to forming an appropriate cavity to a certain analyte.

Commercial precursors 2-quinolinecarbaldehyde **1a** and 8-hydroxy-2-quinolinecarbaldehyde **1b** were stirred in methanol for 8–10 h at room temperature with three different hydrazines (**2a-c**) to yield hydrazones **4a-e**. The reaction mixtures were filtered, and the precipitated compounds were obtained in yields from 52 to 76 %. All the compounds were characterized by FTIR, ^{1}H and ^{13}C NMR, and HRMS. Hydrazones **4f-g** were synthesized as previously reported [29].

The ^{1}H NMR spectra of the new compounds show characteristic hydrazone N–NH protons at 11.34 and 11.40 ppm, for **4a** and **4b**, respectively. This signal appears at 10.81 ppm for compound **4e**. OH signals for **4b** and **4d** appear at 9.67 and 9.56 ppm, respectively. Imine N=CH protons appear between 8.20 and 8.42 ppm for compounds **4a**, **4b**, and **4e**. For compounds **4c-d**, an upfield shift is observed for these signals, appearing at 7.22 and 7.36 ppm, respectively. Regarding ^{13}C NMR spectra, N=CH imine carbon signal appears between 135.5 and 143.2 ppm for all the compounds. Compound **4e** shows the carboxylate group C=O signal at 163.2 ppm. It can also be seen that the compounds with OH group at position 8' (**4b** and **4d**) show a significant downfield shift on C8' (δ between 153.1 and 153.5 ppm), compared to the correspondent derivatives without OH group *e.g.,* **4a** and **4c** (δ between 128.4 and 128.8 ppm).

3.2. Chemosensory studies

The new group of compounds **4a-e**, together with two other previously reported quinoline-based HZ **4f-g** [29], and the two quinoline precursors **1a-b**, were tested in the presence of TBT. A preliminary chemosensory test was carried out with the addition of 50 equiv. of TBT to an ACN solution of each compound (1 mL, 10^{-5} M). Compounds **1b**, **4a**, **4b**, and **4d**, showed colorimetric changes in the presence of TBT. Besides, HZ **4a** showed a fluorimetric change (visible under UV light). To characterize these interactions, spectroscopic and spectrofluorimetric titrations were performed with sequential addition of TBT (10^{-2} M) to a solution of each HZ (10^{-5} M). Fig. 1 shows the spectrophotometric titrations for compounds **1b**, **4a**, **4b**, and **4d**, and the fluorimetric titration for compound **4a**. For compounds **1b**, **4b**, and **4d**, the interactions cause a decrease in the main band of the UV/Visible spectra of HZ, around 339–367 nm, while a new band appears in all cases at 389–457 nm, causing a change of color from colorless to yellow. An inset is shown on all spectra with the absorbance values at the original band wavelength and the new band wavelength, with the sequential addition of TBT. For the interaction between compound **4a** and TBT, a small decrease occurs in the main band at 356 nm, and the appearance of a new band at 512 nm, causing a change of color from colorless to red. The appearance of fluorescence is also caused by this new band; with an excitation at 512 nm HZ **4a** shows the appearance of an emission band at 576 nm, which increases with the sequential addition of TBT (and correspondent increase of the 512 nm absorption band). An inset was also introduced to show the absorbance values at the original band wavelength and the new band wavelength in the case of the spectrophotometric titration – Fig. 1d, and the fluorescence intensity values in the case of the spectrofluorimetric titration – Fig. 1e, with the sequential addition of TBT.

Table 1 shows the photophysical properties of all the tested compounds. When optical changes are observed upon interaction with TBT, the LOD and LOQ are shown in μM. These values were calculated from the linear zone of calibration curves, according to the literature [30]. From all the compounds showing optical changes with the interaction with TBT, the quinoline precursor **1b** is the least sensitive, showing a LOD of 18.9 μM and a LOQ of 62.9 μM. Compounds **4d** and **4b** show LODs of 9.2 and 4.5 μM, respectively. Regarding HZ **4a,** a LOD of 4.8 μM and a LOQ of 15.9 μM were obtained for absorbance changes, while a LOD of 1.7 μM and a LOQ of 5.8 μM were obtained for fluorescence changes. The previous TBT chemosensors reported by Jin and collaborators were able to quantify TBT between 6 and 20 μM [21]. Overall, the novel quinoline-based hydrazones herein reported show the ability to detect this biocide in the same order of concentrations.

3.3. Predictive model of chemosensory ability

The results obtained from compounds **1a**, **1b**, and **4a-4g** show that modifying the chemical environment of the quinoline moiety can influence the compound's ability to trigger some useful response in the presence of TBT. Indeed, some patterns appear to emerge from the data presented in Table 1. For example, the presence of OH group at position 8 usually renders a TBT-sensitive compound, but this rule does not apply to compound **4g**, which has an OH group but does not produce any color

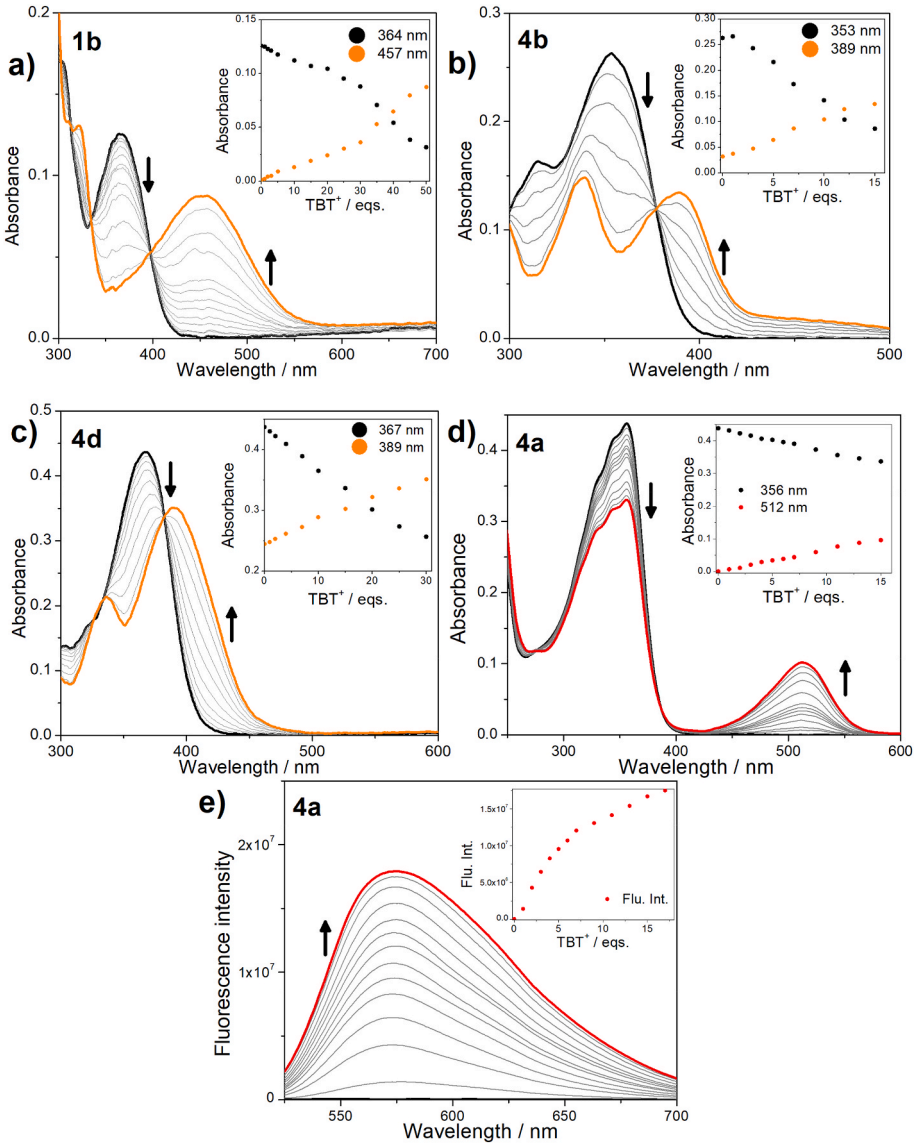

Fig. 1. Spectrophotometric titrations of compounds: **1b** (a); **4b** (b); **4d** (c); **4a** (d), and spectrofluorimetric titration of compound **4a** (e) with TBT. Inset: absorbance and fluorescence values by number of equivalents of TBT added.

Table 1
Photophysical properties of precursors **1a-b**, HZ **4a-g**, and TSC **5a-b**, LOD, and LOQ for the interaction with TBT.

Compound	λ_{abs}/ nm	log ε	LOD_{abs}/μM (LOD_{flu}/ μM)	LOQ_{abs}/μM (LOQ_{flu}/ μM)
1a	289	3.9	–	–
1b	364	4.1	18.9	62.9
4a	356	4.6	4.8 (1.7)	15.9 (5.8)
4b	353	4.4	4.5	15.1
4c	367	4.6	–	–
4d	367	4.6	9.2	30.6
4e	368	4.8	–	–
4f	379[29]	4.5[29]	–	–
4g	385[29]	4.5[29]	–	–
5a[a]	339	4.7	13.8	45.8
5b[a]	345	4.7	3.1	10.4

[a] Compounds **5a** and **5b** were synthesized after the development of the Ridge Regression model, after being signaled as promising chemosensor candidates.

change in the presence of TBT, as shown in Table 1. On the other hand, compound **4a** has some of the lowest detection limits for TBT (Cf. Table 1), despite not having any OH group in its structure. Moreover, the structural diversity of the HZ substituent or the presence of the parent carbonyl group in compounds **1a** and **1b** hindered the proposal of simple structure-based rules. Thus, it has been adopted the hypothesis that the chemosensory ability of a given compound could be predicted from some electronic parameters local to the quinoline moiety. The Ridge classifier method was chosen as it maps the positive and negative cases to the {-1; 1} set and then carries out a linear least squares regression of the explanatory variables, with a L2 regularization, which helps prevent overfitting.

Both the preliminary as well as the final models achieved 100 % accuracy regarding their ability to fit the data concerning the known quinoline and their HZ derivatives. However, the lack of enough experimental data to make a traditional train: test split prompted the authors to test the model by helping generate new compounds. Indeed, the synthesis of TSC **5a** and **5b** was considered as a possible route to expand the compound library, and their structures were subjected to the same DFT and QTAIM treatment detailed for the quinoline and HZ compounds, yielding a positive prediction for the detection of TBT in

both cases.

To validate the model, two novel TSC were synthesized. Compounds **5a** and **5b** were synthesized through the same method using as precursors quinoline carbaldehyde **1a** and hydroxyquinoline carbaldehyde **1b**, with thiosemicarbazide **3a**. Characterization by FTIR, ^{1}H and ^{13}C NMR, and HRMS confirmed the structure of both compounds. The two TSC were tested as TBT chemosensors, and both compounds showed colorimetric changes in the presence of TBT. The results of the spectrophotometric titrations are shown in Fig. 2. Regarding compound **5a**, a decrease in the main band at 339 nm and the appearance of a new band at 412 nm is observed. For compound **5b**, a similar behavior occurred, with the decrease of the main band at 345 nm and the appearance of a new band at 437 nm. The sensitivity of compound **5a** is not very good, showing a LOD of 13.8 μM. However, TSC **5b** is the most sensitive compound in terms of absorption, with a LOD of 3.1 μM and a LOQ of 10.4 μM.

At the end of the feature selection process, the most important features determining a classification of the quinoline and HZ compounds by chemosensing activity were mostly related to the weight of certain atomic contributions to the HOMO. This is highlighted by the high permutation importance score of these variables in the final mode, especially contributions to the HOMO of the atoms at positions 1 (3.3 %), 5 (10 %), 6 (5.5 %), 7 (13 %), and 8 (16 %) of the quinoline core. These results reveal that the contribution of the benzo portion of the quinoline moiety to the HOMO plays an important role in determining the possible sensing activity of these compounds. The permutation importance routine also highlighted the sum of the contributions to the HOMO of all atoms in the quinoline moiety, %HOMO(Q), as an important factor (%PI = 22 %). On the other hand, the atomic contributions to the LUMO were mostly excluded during the feature selection process, with only the LUMO contributions by the atoms in positions 1 and 5 being selected for the final model, and even so, scoring relatively low in the final importance assessment (11 % and 5.5 %, respectively).

The impact of the selected variables in the final model is perhaps better understood in the context of game theory, under the SHAP (SHapley Additive exPlanations) framework, depicted in Fig. 3 for the classification of the validation molecules **5a** (Figs. 3a) and **5b** (Fig. 3b) [40,41]. In both cases, the SHAP visualization of the classification process starts at the classifier's expected response value (E[f(s)] = 0.072, at the bottom of each diagram). In the case of compound **5a** (Fig. 3a) there are some minor contributions pushing the model towards a positive outcome (+0.32), which are then counteracted by the negative contributions provided by the atomic contributions of N1 and C6 to the HOMO. However, the main driver towards a positive classification is the combined contributions given by the weight of atoms C5, C7, and C8 to the HOMO, as well as the overall delocalization index of the HOMO. Finally, the model's expectation towards being in the presence of an active compound is moderated by the weight of the quinoline atoms to the HOMO.

As shown in Fig. 3b, the decision process for compound **5b** is noticeably different to the process described above for compound **5a**. Indeed, the decision process starts with some small positive contributions related to the weight of the atomic orbitals of N1 in either HOMO or LUMO, followed by another small positive contribution generated by % HOMO(C6). This latter contribution already hints at some major differences between the two compounds, as the same variable had a negative contribution in compound **5a**. Delving further into the raw values of this feature, one concludes that small values of % HOMO(C6) gather some momentum towards a positive outcome. The delocalization index of the HOMO is much smaller in **5b** than in **5a** and this decrease in delocalization carries some penalty regarding a positive classification. Indeed, all small positive contributions listed above are almost perfectly canceled by the decrease in the delocalization of the HOMO, as well as the difference in the percentual contribution of the quinoline atoms to the HOMO and LUMO, δ%FMO(Q), and the weight of C8 to the HOMO. Thus, the decision process depicted in Fig. 3b can be summed up by the contributions of two major players: the weight of C5 and the combined weight of the quinoline atoms to the HOMO. Regarding the weight of C5 to the HOMO, it is noteworthy to compare this result with the one depicted for compounds **5a** (Fig. 3a): whereas in the previous case, the small weight of C5 to the HOMO had a moderately high positive contribution to the model's outcome, the hydroxylation of position 8 of the quinoline moiety increased the weight of C5 to the HOMO by almost 30-fold, which has a negative impact on the model's outcome. This is counteracted by the also very high overall contribution of the atoms in the quinoline moiety to the HOMO, which lands the final decision function in the positive realm.

The decision processes illustrated in Fig. 3 indicate the general picture that the increasing cumulative contribution of the quinoline atoms to the HOMO has a positive impact on the prediction of the sensing ability of these quinoline derivatives towards TBT. On the other hand, the increasing contribution of the individual atoms of the benzo submoiety has a negative impact on the model's outcome. Thus, when there are large contributions of the quinoline atoms to the HOMO, this must be in a non-homogeneous manner, with the pyridine sub-moiety being the preferred contributor to the HOMO.

On the other hand, when the overall contribution of the quinoline atoms to the HOMO is low, the small contributions of the atoms in the benzo moiety bear a positive effect on the model's response, so that compounds where the HOMO is not as strongly localized at the quinoline moiety, benefit from having whatever small weight of the quinoline contribution centered in the atoms of the benzo sub-unit. What is more, the hydroxylation of position 8 of the quinoline moiety appears to increase the HOMO contribution of C8 and C5 to the HOMO. Thus, the

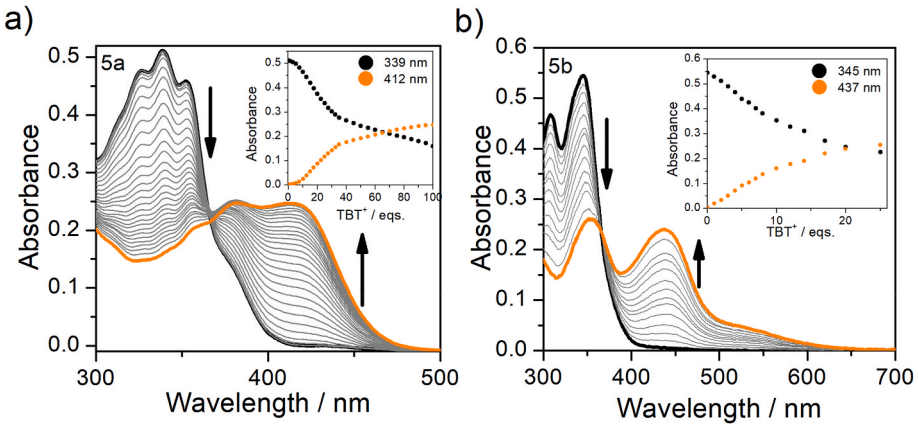

Fig. 2. Spectrophotometric titrations of compounds **5a** (a) and **5b** (b) with TBT. Inset: absorbance values by number of equivalents of TBT added.

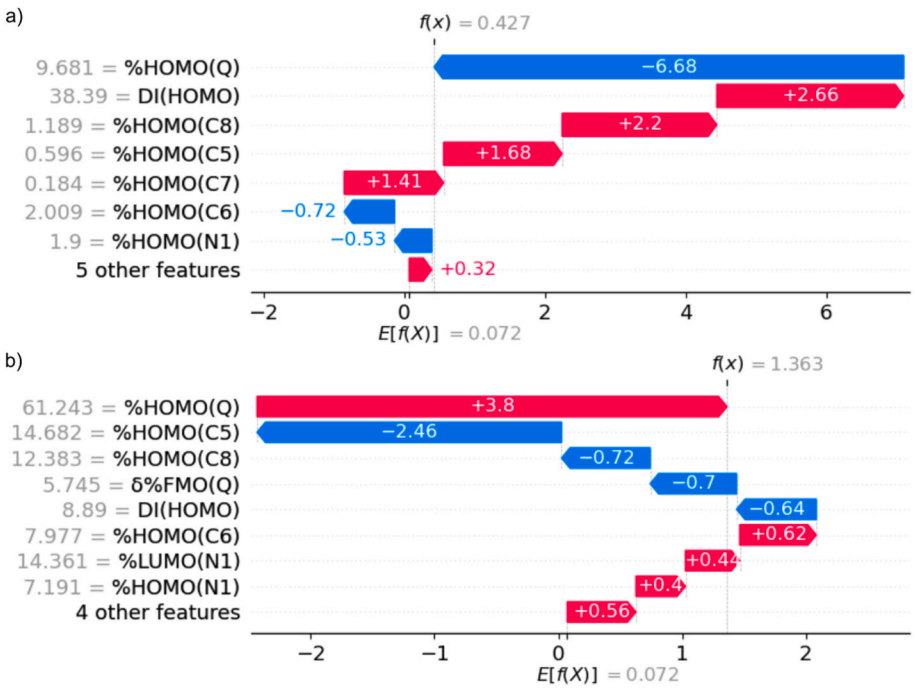

Fig. 3. SHAP waterfall diagrams illustrating the decision process for the prediction of chemosensing activity of TSC **5a** (a) and **5b** (b). Grey values at the side of each feature name provide the numerical value of each feature, E[f(X)] represents the model's expected outcome, and f(x) represents the model's outcome for each compound (*i.e.*, the model's expectation value for the data, considering that −1 represents a compound without sensing ability towards TBT, and +1 a compound with sensing ability).

introduction of a hydroxyl group at C8 is beneficial only if the overall increase in the contribution of the quinoline moiety to the LUMO outweighs this increase in the weight of the benzo sub-moiety. This may be achievable, for example, if the orbitals of the group at the other end of the hydrazone or thiosemicarbazone linkage are unable to interact with the frontier molecular orbitals of the quinoline fragment.

4. Conclusions

This work reports the synthesis of five novel HZ based on a quinoline moiety, by straightforward condensation reactions between aldehyde and hydrazine precursors, with yields ranging from 52 to 76 %. The group of compounds including the five new compounds plus the two quinoline carbaldehyde precursors and two other previously reported HZ [29], were designed to be tested as TBT optical chemosensors. Preliminary sensory tests were carried out, showing compounds **1b**, **4a**, **4b**, and **4d** exhibited colorimetric or fluorimetric changes in the presence of TBT. The interaction between these compounds and TBT was tested by spectrophotometric or spectrofluorimetric titrations, and LODs and LOQs were calculated. The results show the fluorimetric detection of TBT by compound **4a** is the most sensitive chemosensing method, judging by the LOD value of 1.7 μM.

The modification of the chemical environment of the quinoline moiety was shown to influence the compound's ability to detect TBT. The Ridge classifier model was developed through some patterns identified on the previously obtained results, and the synthesis of TSC **5a** and **5b** was considered as a possible route to expand the compound library as well as a validation of the model. These two compounds, obtained from aldehyde and thiosemicarbazide precursors, also showed colorimetric changes in the presence of TBT, with LODs of 13.8 and 3.1 μM, respectively. The developed model suggests that the chemosensory ability is related to the weight balance of the pyridine and benzo subunits of the quinoline moiety to the HOMO and appears to be a promising model for the development of further TBT chemosensors with improved sensitivity.

CRediT authorship contribution statement

Rui P. C. L. Sousa: Conceptualization, Formal analysis, Investigation, Methodology, Writing – original draft, Writing – review & editing. **Filipe Teixeira:** Conceptualization, Formal analysis, Investigation, Methodology, Software, Writing – original draft, Writing – review & editing. **Susana P. G. Costa:** Conceptualization, Formal analysis, Funding acquisition, Project administration, Resources, Supervision, Writing – review & editing. **Rita B. Figueira:** Conceptualization, Formal analysis, Funding acquisition, Project administration, Resources, Supervision, Writing – review & editing. **M. Manuela M. Raposo:** Conceptualization, Formal analysis, Funding acquisition, Project administration, Resources, Supervision, Writing – review & editing.

Declaration of competing interest

The authors declare that they have no known competing financial interests or personal relationships that could have appeared to influence the work reported in this paper.

Data availability

Data will be made available on request.

Acknowledgments

Thanks are due to Fundação para a Ciência e Tecnologia (FCT) and FEDER (European Fund for Regional Development)-COMPETE-QRENEU for financial support through the Chemistry Research Centre of the University of Minho (Ref. CQ/UM UID/QUI/00686/2020), and a PhD grant to R. P. C. L. Sousa (SFRH/BD/145639/2019). The NMR spectrometer Bruker Avance III 400 is part of the National NMR Network (PTNMR) and is partially supported by Infrastructure Project No 022161 (co-financed by FEDER through COMPETE 2020, POCI and PORL and FCT through PIDDAC). This work was developed with the support of

computing facilities provided by the Project "Search-ON2: Revitalization of HPC infrastructure of UMinho" (NORTE-07-0162-FEDER-000086), co-funded by the North Portugal Regional Operational Programme (ON.2 – O Novo Norte), under the National Strategic Reference Framework (NSRF), through the European Regional Development Fund (ERDF).

Abbreviations

ACN	Acetonitrile
DFT	Density Functional Theory
FTIR	Fourier-Transformed Infra-Red
GC-MS	Gas Chromatography – Mass Spectrometry
HOMO	Highest Occupied Molecular Orbital
HRMS	High Resolution Mass Spectrometry
HZ	Hydrazone
LC-MS	Liquid Chromatography – Mass Spectrometry
LOD	Limit of Detection
LOQ	Limit of Quantification
LUMO	Lowest Unoccupied Molecular Orbital
NMR	Nuclear Molecular Resonance
QTAIM	Quantum Theory of Atoms In Molecules
SHAP	SHapley Additive exPlanations
TBT	Tributyltin
TLC	Thin Layer Chromatography
TSC	Thiosemicarbazone

Appendix A. Supplementary data

Supplementary data to this article can be found online at https://doi.org/10.1016/j.dyepig.2024.112053.

References

[1] Figueira RB, Sousa R, Silva CJR. In: Makhlouf ASH, Abu-Thabit NY, editors. Advances in smart coatings and thin films for future industrial and biomedical engineering applications. Amsterdam, Netherlands: Elsevier; 2020. p. 57–97.
[2] Price S, Figueira R. Corrosion protection systems and fatigue corrosion in offshore wind structures: current status and future perspectives. Coatings 2017;7:25.
[3] Sousa RPCL, Figueira RB, Costa SPG, Raposo MMM. Optical fiber sensors for biocide monitoring: examples, transduction materials, and prospects. ACS Sens 2020;5:3678–709.
[4] Abbott A, Abel PD, Arnold DW, Milne A. Cost-benefit analysis of the use of TBT: the case for a treatment approach. Sci Total Environ 2000;258:5–19.
[5] Dafforn KA, Lewis JA, Johnston EL. Antifouling strategies: history and regulation, ecological impacts and mitigation. Mar Pollut Bull 2011;62:453–65.
[6] Schultz MP, Bendick JA, Holm ER, Hertel WM. Economic impact of biofouling on a naval surface ship. Biofouling 2011;27:87–98.
[7] Li Y, Ning C. Latest research progress of marine microbiological corrosion and biofouling, and new approaches of marine anti-corrosion and anti-fouling. Bioact Mater 2019;4:189–95.
[8] Hardy FG. Fouling on North sea platforms. Bot Mar 1981;24:173–6.
[9] Apolinario M, Coutinho R. Advances in marine antifouling coatings and technologies. Cambridge, UK: Woodhead Publishing Limited; 2009. p. 132–47.
[10] Antizar-Ladislao B. Environmental levels, toxicity and human exposure to tributyltin (TBT)-contaminated marine environment - a review. Environ Int 2008;34:292–308.
[11] Luan TG, Jin J, Chan SMN, Wong YS, Tam NFY. Biosorption and biodegradation of tributyltin (TBT) by alginate immobilized *Chlorella vulgaris* beads in several treatment cycles. Process Biochem 2006;41:1560–5.
[12] Berge JA, Brevik EM, Bjørge A, Følsvik N, Gabrielsen GW, Wolkers H. Organotins in marine mammals and seabirds from Norwegian territory. J Environ Monit 2004;6:108–12.
[13] Ohji M, Arai T, Miyazaki N. Comparison of organotin accumulation in the masu salmon *Oncorhynchus masou* accompanying migratory histories. Estuar Coast Shelf Sci 2007;72:721–31.
[14] Ohji M, Arai T, Miyazaki N. Acute toxicity of tributyltin to the Caprellidea (Crustacea: Amphipoda). Mar Environ Res 2005;59:197–201.
[15] Laranjeiro F, Sánchez-Marín P, Oliveira IB, Galante-Oliveira S, Barroso C. Fifteen years of imposex and tributyltin pollution monitoring along the Portuguese coast. Environ Pollut 2018;232:411–21.
[16] Artifon V, Castro ÍB, Fillmann G. Spatiotemporal appraisal of TBT contamination and imposex along a tropical bay (Todos os Santos Bay, Brazil). Environ Sci Pollut Res 2016;23:16047–55.
[17] Matthiessen P, Gibbs PE. Critical appraisal of the evidence for tributyltin-mediated endocrine disruption in mollusks. Environ Toxicol Chem 1998;17:37–43.
[18] Mikac N, Turk MF, Petrović D, Bigović M, Krivokapić S. First assessment of butyltins (BuTs) contamination of the Montenegrin coast (Southeast Adriatic): tributyltin (TBT) poses a threat to the marine ecosystem. Mar Pollut Bull 2022;185:114270.
[19] Filipkowska A, Kowalewska G. Butyltins in sediments from the Southern Baltic coastal zone: is it still a matter of concern, 10 years after implementation of the total ban? Mar Pollut Bull 2019;146:343–8.
[20] Concha-Graña E, Moscoso-Pérez C, Fernández-González V, López-Mahía P, Gago J, León VM, Muniategui-Lorenzo S. Phthalates, organotin compounds and per-polyfluoroalkyl substances in semiconfined areas of the Spanish coast: occurrence, sources and risk assessment. Sci Total Environ 2021;780:146450.
[21] Jin X, Hao L, She M, Obst M, Kappler A, Yin B, Liu P, Li J, Wang L, Shi Z. Visualizing tributyltin (TBT) in bacterial aggregates by specific rhodamine-based fluorescent probes. Anal Chim Acta 2015;853:514–20.
[22] Chen W, Liang H, Wen X, Li Z, Xiong H, Tian Q, Yan M, Tan Y, Royal G. Synchronous colorimetric determination of CN^-, F^-, and $H_2PO_4^-$ based on structural manipulation of hydrazone sensors. Inorg Chim Acta 2022;532:120760.
[23] Wu WN, Wu H, Wang Y, Mao XJ, Liu BZ, Zhao XL, Xu ZQ, Fan YC, Xu ZH. A simple hydrazone as a multianalyte (Cu^{2+}, Al^{3+}, Zn^{2+}) sensor at different pH values and the resultant Al^{3+} complex as a sensor for F^-. RSC Adv 2018;8:5640–6.
[24] Khattab TA, Gaffer HE. Synthesis and application of novel tricyanofuran hydrazone dyes as sensors for detection of microbes. Color Technol 2016;132:460–5.
[25] Yang Y, Gao CY, Liu J, Dong D. Recent developments in rhodamine salicylidene hydrazone chemosensors. Anal Methods 2016;8:2863–71.
[26] Raposo MMM, García-Acosta B, Ábalos T, Calero P, Martínez-Máñez R, Ros-Lis JV, Soto J. Synthesis and study of the use of heterocyclic thiosemicarbazones as signaling scaffolding for the recognition of anions. J Org Chem 2010;75:2922–33.
[27] Santos-Figueroa LE, Moragues ME, Raposo MMM, Batista RMF, Costa SPG, Ferreira RCM, Sancenón F, Martínez-Máñez R, Ros-Lis JV, Soto J. Synthesis and evaluation of thiosemicarbazones functionalized with furyl moieties as new chemosensors for anion recognition. Org Biomol Chem 2012;10:7418–28.
[28] Santos-Figueroa LE, Moragues ME, Raposo MMM, Batista RMF, Ferreira RCM, Costa SPG, Sancenón F, Martínez-Máñez R, Soto J, Ros-Lis JV. Synthesis and evaluation of fluorimetric and colorimetric chemosensors for anions based on (oligo)thienyl-thiosemicarbazones. Tetrahedron 2012;68:7179–86.
[29] Sousa RPCL, Costa SPG, Figueira RB, Raposo MMM. New dinitrophenyl hydrazones as colorimetric probes for anions. Chemosensors 2022;10:384.
[30] Thomsen V, Schatzlein D, Mercuro D. Limits of detection in spectroscopy. Spectroscopy 2003;18:103.
[31] Becke AD. A new mixing of Hartree–Fock and local density-functional theories. J Chem Phys 1993;98:1372–7.
[32] Weigend F, Ahlrichs R. Balanced basis sets of split valence, triple zeta valence and quadruple zeta valence quality for H to Rn: design and assessment of accuracy. Phys Chem Chem Phys 2005;7:3297–305.
[33] Grimme S, Ehrlich S, Goerigk L. Effect of the damping function in dispersion corrected density functional theory. J Comput Chem 2011;32:1456–65.
[34] Grimme S, Antony J, Ehrlich S, Krieg H. A consistent and accurate ab initio parametrization of density functional dispersion correction (DFT-D) for the 94 elements H-Pu. J Chem Phys 2010;132:154104. https://doi.org/10.1063/1.3382344.
[35] Neese F, Wennmohs F, Becker U, Riplinger C. The ORCA quantum chemistry program package. J Chem Phys 2020;152:224108.
[36] Lu T, Chen F. Multiwfn: a multifunctional wavefunction analyzer. J Comput Chem 2012;33:580–92.
[37] Pedregosa F, Varoquaux G, Gramfort A, Michel V, Thirion B, Grisel O, Blondel M, Prettenhofer P, Weiss R, Dubourg V, Vanderplas J, Passos A, Cournapeau D, Brucher M, Perrot M, Duchesnay É. Scikit-learn: machine learning in python. J Mach Learn Res 2011;12:2825–30.
[38] Noorizadeh S, Shakerzadeh E. Shannon entropy as a new measure of aromaticity, Shannon aromaticity. Phys Chem Chem Phys 2010;12:4742–9.
[39] Breiman L. Random forests, Mach. Learn. 2001;45:5–32.
[40] Bach S, Binder A, Montavon G, Klauschen F, Müller KR, Samek W. On pixel-wise explanations for non-linear classifier decisions by layer-wise relevance propagation. PLoS One 2015;10:e0130140.
[41] Lundberg SM, Lee S-I. In: Garnett IG, Luxburg UV, Bengio S, Wallach H, Fergus R, Vishwanathan S, editors. Advances in neural information processing systems 30. Curran Associates, Inc.; 2017. p. 4765–74.
[42] Yu Y, Hou J, Yu L, Yang Y, Wang C. Lattice modulation effect of liquid–solid interface on peptide assemblies. Surf Sci 2016;649:34–8.
[43] Farshbaf S, Anzenbacher P. Fluorimetric sensing of ATP in water by an imidazolium hydrazone based sensor. Chem Commun 2019;55:1770–3.
[44] Xu H, Wang X, Zhang C, Wu Y, Liu Z. Coumarin-hydrazone based high selective fluorescence sensor for copper(II) detection in aqueous solution. Inorg Chem Commun 2013;34:8–11.
[45] Jabeen M. A comprehensive review on analytical applications of hydrazone derivatives. J. Turkish Chem. Soc. Sect. A Chem. 2022;9:663–98.